

SMART SPINDLES: INSTRUMENTATION FOR PROCESS MONITORING

Eric Marsh¹, R. Ryan Vallance²

¹Department of Mechanical Engineering
Penn State University
University Park, PA, USA

²Department of Mechanical Engineering
The George Washington University
Washington, DC, USA

INTRODUCTION

Two schools of thought exist regarding the relationship of cutting force versus MRR in grinding. Snoeys et al. and Malkin [1, 2] argue for an exponential relationship of the form:

$$F'_n = F_1 \left(\frac{2\pi r_w \dot{u}}{v_g} \right)^f \quad (1)$$

with F_1 and f constant. Others, beginning with Lindsay and Hahn [3], and more recently Razavi et al. and Kurfess et al. [4, 5] suggest a linear relationship:

$$F'_n = \frac{2\pi r_w \dot{\delta}_w}{\Lambda} \quad (2)$$

This paper will show that during the first part of spark-in, when plowing and sliding dominate [2], material removal is essentially zero, and neglecting plowing and sliding will still lead to a reasonably accurate model.

Chen et al. [6] neglect wheel wear and assume the normal grinding force is directly proportional to the actual depth of cut. "Depth of cut" is defined as the difference between the current infeed position and the infeed position one revolution prior. The assumption of the force proportionality neglects force contributions due to plowing and sliding, i.e. $F_{n,sl} = F_{n,pl} = 0$. Chen calculates the following equations for modeling the grinding system [6, 7]:

$$F_n = K_c \cdot a = K_c \cdot \frac{\dot{\delta}_w}{\omega_w} \quad (3)$$

where K_c is the grinding contact coefficient.

The equation of motion is defined as

$$\ddot{\delta}_w = \frac{k_e \cdot \omega_w}{K_c} (\dot{u} - \dot{\delta}_w) \quad (4)$$

Defining $\tau = \frac{K_c}{k_e \omega_w}$, the part size at any time t , the solution is:

$$\delta_w = \dot{u} \cdot (t - \tau + \tau \cdot e^{-t/\tau}) \quad (5)$$

and

$$\dot{\delta}_w = \dot{u}(1 - e^{-t/\tau}) \quad (6)$$

It is possible to develop a relationship between F_n , u , and τ . This allows calculation of the grinding time constant using easily-measured variables:

$$F_n = \frac{K_c \dot{u}(1 - e^{-t/\tau})}{\omega_w} \quad (7)$$

The grinding contact coefficient K_c is dependent on the grinding contact width b , so it is often given as K'_c independent of width, in the form:

$$K'_c = \frac{K_c}{b} \quad (8)$$

After determining τ as a function of commanded infeed velocity and normal force, it is a simple matter to calculate δ_w using F_n , u , and dwell time during spark-out. This calculation could be run real-time to accurately control the grinding process. The following experiments prove the validity of the theoretical model, allowing precise, repeatable part creation using machine infeed and normal force measurements.

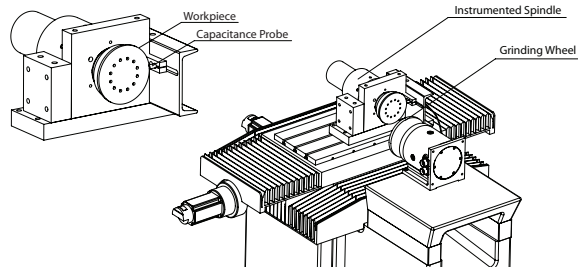


FIGURE 1. Moore CNC grinder with a Professional Instruments BLOCK-HEAD instrumented work spindle with embedded capacitive probes from Lion Precision along with a second PI grinding wheel spindle.

GRINDING INSTRUMENTATION

High-quality results demand high-quality equipment and rigorous vetting to prove its worthiness. The hardware used in this paper allows flexibility in experimentation and conclusions about a wide variety of observations about grinding dynamics.

The instrumented spindle, developed by Professional Instruments for high-accuracy force measurement in any environment, uses four high-precision capacitance probes mounted inside a motorized 4R BLOCK-HEAD spindle. The probes are imbedded in the spindle stator, facing the spindle thrust plate as the inset shows in Figure 1. Manufactured by Lion Precision, the probes have a sensitivity of $1 \text{ V}/\mu\text{m}$ and a range of $20 \mu\text{m}$. The probes are perfectly suited for this application, as the air pressure keeps out external contaminants and the 4R spindles are very stiff ($79.08 \text{ N}/\mu\text{m}$ for force application 100 mm from spindle centerline).

In addition to the two capacitance probes measuring grinding forces, one probe faces the ground surface of the part and another measures a reference point on the CNC table. In an industrial application, these probes are not likely to see use, as the part sensor is too exposed and the table motion is measured internally by the CNC machine.

The ability to acquire repeatable data is useless without a method for transforming it into a useful quantity for interpretation. The National Instruments PCI-6110E data acquisition card converts the analog signal to a 12-bit digital one, once the signal is filtered at 1 kHz using a fourth-order Butterworth LPF. This level of filtering, when used with a sampling frequency of 5.12 kHz (1024 samples/revolution at 300 rpm), is well below the

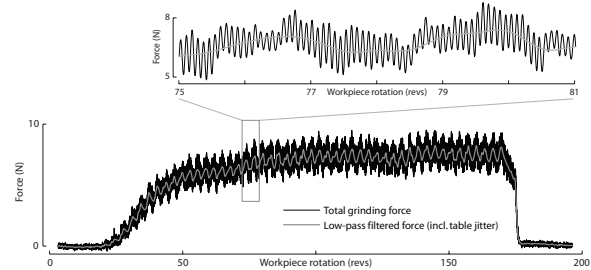


FIGURE 2. Comparison of the normal force data before and after aggressive wavelet filtering

Nyquist frequency and avoids losing too much information. All data processing other than the ADC is currently performed in post-processing, using MATLAB. The post-processing software removes the synchronous thrust plate form error and uses a Yule-Walker low-pass filter with a cutoff frequency of 25 undulations per revolution (upr). It also corrects for thermal drift due to heating of the workpiece spindle using a second-order curve fit.

RESULTS

Aggressive wavelet filtering of the normal grinding force shows several important attributes of the grinding process in Figure 2. The two effects that stand out most prominently are the overarching grinding force growth, and the higher-frequency, low-amplitude vibration superposed upon the former. The force fluctuation can be traced to machine feed axis jitter resulting from the low infeed rate. Better tuning of the machine hardware gains specifically for low-infeed grinding could result in reduction of the force fluctuation. Even so, the slight fluctuations do little to detract from the overall effect of the grinding force. In the inset plot showing a close-up of two revolutions, the higher-frequency force effects are clearly visible.

The force measurement alone yields very interesting conclusions, shown for one plunge cycle in Figure 3. The three-dimensional plot shows a lobed pattern throughout the grinding process. The approximately eleven-lobe pattern is caused by the relationship between the wheel and workpiece speeds. Places where the lobes appear to precess are caused by non-constant wheel and workpiece spindle motor speeds. At the beginning of grinding contact, the shape of the workpiece is indirectly observable. For out-of-center parts, a single sinusoidal wave with a period equal to one revolution is apparent, while for parts that are centered but have some sort of form error, a higher-frequency wave is seen. In this case,

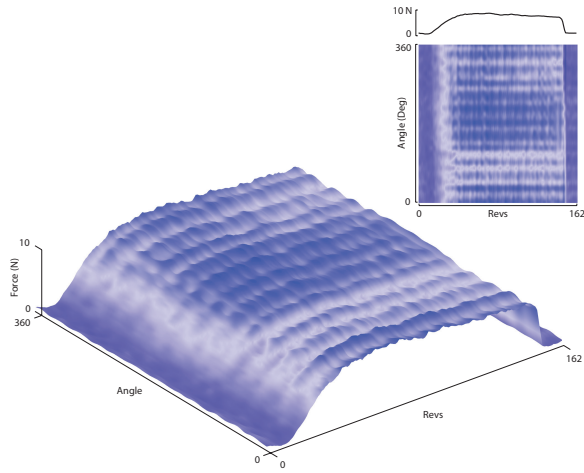


FIGURE 3. Normal grinding force F_n during one plunge cycle with 162 workpiece revolutions.

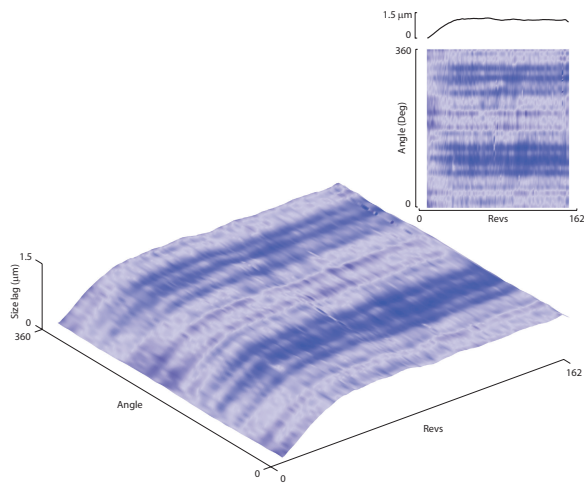


FIGURE 4. Lag between commanded infeed u and part diameter δ_w .

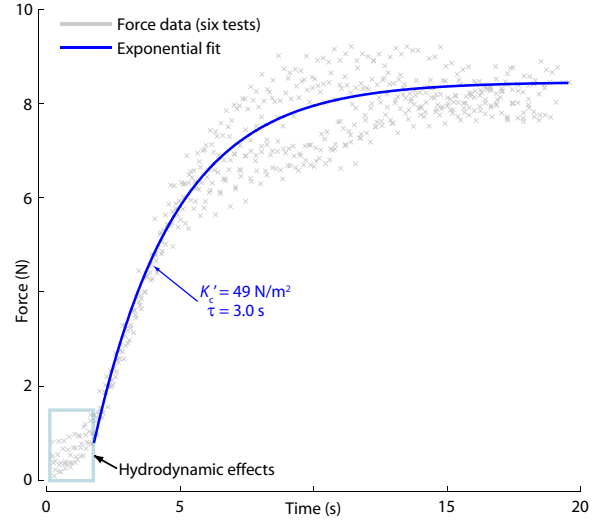


FIGURE 5. Comparison between the normal force model and the force measured during experimentation. Accuracy of the model improves with removal of the hydrodynamic effect observed just before grinding commences.

the dominant eleven peaks show the dependence of part shape upon the relationship $\frac{\omega_g}{\omega_w}$.

Figure 4 shows a plot of the difference between the commanded infeed and the part removal during grinding, representing the amount by which the part removal lags the commanded infeed. The increasing magnitude shows the system compliance during spark-in, which eventually reaches its steady-state value. This view also validates Equation 5 by demonstrating the exponential relationship between u and δ_w . The two-lobe shape is the dominant grinding frequency after the wheel-workpiece speed ratio, is seen as two darker bands on the surface of the plot.

Verification of the accuracy of the assumed model then permits the application of the grinding algorithm described in the Introduction. The operator first measures the workpiece offline and determines the amount of material removal required to obtain the correct tolerance. This value is fed into Equation 5, which returns the grinding time t . This is only an intermediate step, since the operator does not know the moment at which grinding begins. The calculation of a threshold grinding force at which the part reaches the desired size allows easy process monitoring, so the grinding time is next plugged into Equation 7 using the values of K_c and τ determined from initial system characterization. The normal force output is the point at

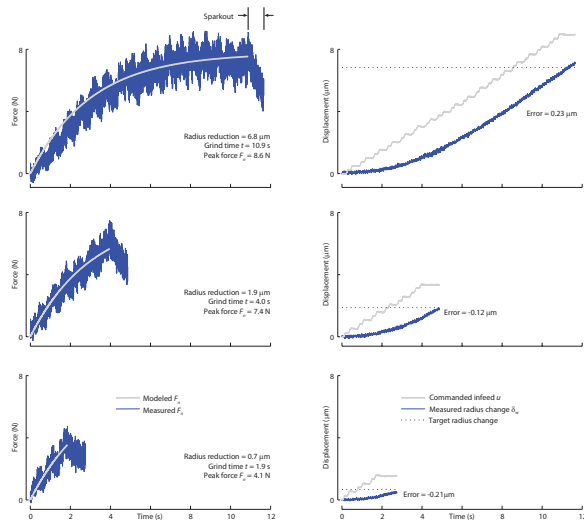


FIGURE 6. The operator determines the part radius reduction required to obtain the desired tolerance, which is then used to calculate the threshold normal force from the grinding time. Once the threshold force is reached the part can be immediately retracted, or be subject to some spark-out. The tests in this paper included real-time measurement of the part radius to prove the accuracy of the model. Comparison between the target radial change and the achieved are shown.

which the operator will retract the part or begin spark-out, depending on surface finish requirements. Figure 6 shows this process graphically, comparing the grinding force model to the actual results as well as showing the error between the desired part size and the result.

The force-dependent grinding algorithm works best for very small infeed depths. For depths which result in grinding forces approaching the steady-state value, small differences in the grinding force can result in gross part size errors. While a small force spike in the first few seconds of grinding might only result in a part error of a few tenths of a micrometer, once the force has stabilized it might cut several seconds off the process, causing several full micrometers of error. On the test rig used here, the process works best for infeed depths below $8 \mu\text{m}$. With the accuracy and stiffness of modern machines, traditional methods can be employed to reduce the part size to within that amount, after which the finish pass can be performed.

CONCLUSION

Grinding is a complex process, and even slight changes in certain variables can drastically

change the wheel-workpiece interaction. Real-time measurement of grinding forces and the part size change allow insight into the nature of the process, improving every facet of grinding technology. The grinding algorithm discussed in this paper allows repeatable creation of ground parts of the highest quality by characterizing the system with a few simple measurements and then monitoring the normal grinding force during in-process. This method reduces cost by improving yield and minimizing iterations to reach the desired part size. It works especially well for finish passes with low infeed rates. Lower-tolerance grinding applications can still get by with traditional iterative grinding methods. The point at which an operator should switch to the method described here is when the remaining material is less than the amount of machine compliance during operating conditions. As an added bonus, the instruments used to gather this data are nearly immune to the harsh environs of the industrial grinding sector.

REFERENCES

- [1] Snoeys R, Peters J, Decneut A. Significance of chip thickness in grinding. *Annals of the CIRP*. 1974;23(2):227–237.
- [2] Malkin S. *Grinding Technology: Theory and Applications of Machining with Abrasives*. 1st ed. Ellis Horwood Limited; 1989.
- [3] Lindsay RP, Hahn RS. On the basic relationships between grinding parameters. *Annals of the CIRP*. 1971;19(4):657–66.
- [4] Razavi HA, Kurfess TR, Danyluk S. Force control grinding of gamma titanium aluminide. *International Journal of Machine Tools and Manufacture*. 2003;43(2):185–191.
- [5] Kurfess TR, Whitney DE, Brown ML. Verification of a dynamic grinding model. *Journal of Dynamic Systems, Measurement and Control, Transactions ASME*. 1988;110(4):403–409.
- [6] Chen X, Allanson D, Thomas A, Moruzzi JL, Rowe WB. Simulation of feed cycles for grinding between. *International Journal of Machine Tools & Manufacture*. 1994;34(5):603–616.
- [7] Chen X, Allanson DR, Rowe WB. Life cycle model of the grinding process. *Computers in Industry*. 1998;36(1-2):5–11.